



Application of the metallized titanate nanorod in the photodegradation of methyl orange

Sana Ben Moussa¹

Received: 3 July 2023 / Accepted: 24 July 2023 / Published online: 2 August 2023
© Akadémiai Kiadó, Budapest, Hungary 2023

Abstract

The aim of this work is to study the catalytic activity of titanate nanorods materials doped by platinum and gold nanoparticles in the photodegradation reaction of methyl orange. Nanorods are metallized by deposition precipitation with urea and impregnation at 2 wt% of metal. The characteristics of materials are determined using the following methods: photoelectron spectroscopy, transmission electron microscopy, UV–Vis in reflection diffuse (RDS/UV–Vis), X-ray diffraction, N₂ adsorption–desorption and ICP analysis. The results of characterization proved the formation of nanorods structure using hydrothermal method and an almost total homogeneous deposition of the metallic nanoparticles on the nanorod surface. All materials are used in the photodegradation of organic pollutant dye (methyl orange) under UV or visible irradiations. Pt doped nanorods shows the best catalytic activity in the photodegradation of dye. The conversion and mineralization rates achieved 100 and 78%, respectively.

Keywords Platinum · Gold · Nanoparticles · Photodegradation · Methyl orange

Introduction

Organic compounds in wastewater, such as dyes and pigments in industry effluents and recently pharmaceutical wastes are toxic, mutagenic and carcinogenic. They present a real danger on aquatic living and humans. Dyes are an example of pollutants released in the environment in significant proportions and difficult to eliminate [1–3]. Several methods to resolve this problem have been reported, including adsorption, coagulation and ultrafiltration but these techniques cannot resolve the problem completely [4, 5]. Since several years, the Advanced Oxidation Processes (AOP) appears as innovative water treatment technologies. Among these AOP,

✉ Sana Ben Moussa
moussasanaa300@gmail.com

¹ Department of Chemistry, Faculty of Science and Arts, King Khalid University, Mohail Assir, Abha, Saudi Arabia

heterogeneous photocatalysis employing semiconductor photocatalysts to degrade dye wastewater is an environmentally friendly technology [4–10]. The aim of the photocatalytic process is to break the big organic dye molecules into simple molecules such as carbon dioxide, water and inorganic (biodegradable intermediates) [11]. Titanium dioxide (TiO_2) has been widely used and investigated for photochemical purposes, due to the stability of its chemical structure, optical and electronic properties, low cost, non-toxicity and especially its photocatalytic features [12–14]. Typically, TiO_2 can only respond in the ultraviolet region due to its wide band gap (around 3.2 eV). Only a small UV fraction of solar light (3–5%) can be used. Therefore, the improvement of titanium dioxide photocatalytic activity is important to extend it in the visible region, usually by the decrease of the band gap [15–18]. Deposition of noble metals such as Pt and Au on the surface of TiO_2 improves its photocatalytic activity [12, 19, 20]. Hernández et al. [12] reported that doping TiO_2 by Au and Pt can change its properties and also the band gap energy. The catalytic activity of Ag_3VO_4 doped TNR (average diameter of about 50–150 nm) exhibit a higher photocatalytic activity for the decomposition of gaseous toluene compared to pure TNR under visible light irradiation. The conversion of toluene over 1% $\text{Ag}_3\text{VO}_4/\text{TNR}$ achieved 70% after 4 h under visible light irradiation. This important activity was related to the strong absorption of this catalyst in visible-light region and excellent charge separation characteristics [21]. It was evoked that the active species involved in the photocatalytic degradation of toluene were: OH^\bullet and $\text{O}_2^{\bullet-}$ radicals. The introduction of the dopant Ag_3VO_4 can improve the spectral response of TiO_2 from the UV to visible region [21]. In the same reaction, the black NiO/TNR (with an average diameter of ~180 nm) exhibit 80% of photodegradation conversion and 56% of mineralization efficiency, which are 7.9 and 4.5 times higher than those of TNR. Detailed characterizations reveal that highly dispersed NiO and p–n heterojunction effectively facilitate light-harvesting, separation and transfer of photo-generated charge carries, and significantly inhibit the recombination of electrons and holes. Furthermore, the realignment of band structure and the p–n heterojunctions in NiO/TNR result in the production of $\text{O}_2^{\bullet-}$ and h^+ with a longer lifetime, which could efficiently attack the aromatic ring of toluene. The efficient adsorption of toluene by H-bonding formation also facilitates the photo-oxidation of toluene on NiO/TNR [22].

In the present study we will study the effect of the preparation method on the production of nanorods from commercial anatase. These nanostructures will subsequently be used as a support for metallic nanoparticles (gold and platinum). The prepared catalysts are: titanate nanorods (TNR), monometallic catalysts: Au/TNR , Pt/TNR and bimetallic catalyst ($\text{Au-Pt}/\text{TNR}$). The obtained catalysts are used in the photodegradation of methyl orange which is a model pollutant used as a dye in industry.

Materials

TiO_2 (anatase), NaOH , HCl , $\text{Pt}(\text{NH}_3)_4(\text{NO}_3)_2$ (purity 99.995%, sigma Aldrich), HAuCl_4 (10 g L^{-1}) (99.99% sigma Aldrich).

Preparation of catalysts

TNR are prepared by hydrothermal treatment method using TiO_2 (anatase) as the raw material. Briefly, 4 g of titania is mixed with 50 mL of NaOH (10 M) and aged used ultrasound bath during 10 min. The mixture is then transferred in a Teflon flask and then the temperature is reported to 180 °C during 48 h. the obtained solid is then washed several times with distilled water, neutralized by a solution of HCl and finally washed with distilled water to eliminate the undesired ions (Cl^- , Na^+). Doping TNR is realized using different ways; for gold-based catalyst, Au is doped using conventional homogenous deposition precipitation. However, the platinum is introduced to Pt/TNRS catalyst using impregnation. Pt/TNR is prepared by dissolving 0.02 g of platinum precursor ($\text{Pt}(\text{NH}_3)_4(\text{NO}_3)_2$) in ultrapure water, then for this solution into a beaker which contains 0.99 g of TNR. This mixture is stirred for 2 h at room temperature. Then, the evaporation of the solvent is carried out in a sand bath (60 °C) for about 5 h, followed by drying in an oven (120 °C) for 24 h and finally calcination of the catalyst at 500 °C for 2 h.

Characterization methods

Surface characterization by photoelectron spectroscopy (XPS) is realized on a SPECS spectrometer, using constant pass energy of 40 eV. The spectrometer main chamber is fixed at $5\text{--}6 \times 10^{-10}$ bar, and the machine is connected with a PHOIBOS 150 9MCD hemispherical electron analyzer, using Al K_{α} (h μ) 1486.6 eV at 250 W and 12.5 kV. Zn $2p_{3/2}$ signal (1022.4 eV) is employed as the internal energy reference in all experiences. The photoelectron spectra are analyzed using Casa-XPS software. The effective contents of Au and Pt in the catalysts are determined by ICP chemical analysis. X-ray diffraction (XRD) is conducted on MiniFlex II diffractometer irradiated with Cu K_{α} radiation, scanning speed of 0.01° and acquisition time 2° min⁻¹. The transmission electron microscopy (TEM) analysis of the catalysts is performed in a JEE-2200FS transmission electron microscope operated with an accelerating voltage of 150 kV. The Diffuse Reflectance UV–Visible analyses (DRS/UV–Vis) are realized using Varian spectrometer model Cary 100 operational with an integrating sphere using BaSO_4 as reference. The N_2 adsorption–desorption isotherms are realized using 3Flex instrument (Micromeritics). The catalysts are degassed at a temperature of 250 °C under N_2 gas all the night.

Photodegradation of methyl orange

The photocatalytic performances of the prepared catalysts are evaluated in the degradation of methyl orange (MO) under different irradiations. Photocatalytic tests are carried out using a discontinuous batch system, which includes a 250 mL Pyrex reactor enveloped by aluminum foil, filled with an aqueous suspension (100 mL) containing 20 mg L⁻¹ of MO and the photocatalyst (1 g L⁻¹). The tests are carried out with an Osram Ultra-Vitalux (300 W) with a sun-like spectrum and a main line

Table 1 Textural and optical characteristics of the studied materials

| Samples | S _{BET} (m ² g ⁻¹) | Total volume pores (cm ³ g ⁻¹) | Eg(eV) |
|----------|--|---|--------|
| TNR | 186 | 0.54 | 2.05 |
| 2%Pt/TNR | 181 | 0.40 | 1.69 |
| 2%Au/TNR | 183 | 0.45 | 2.09 |

Table 2 Chemical composition of the prepared solids determined by ICP chemical analysis

| Materials | Metal _{theoretical} (wt%) | Pt (wt%) | Au (wt%) |
|-----------|------------------------------------|----------|----------|
| Pt/TNR | 2 | 1.98 | – |
| Au/TNR | 2 | – | 1.92 |

in the visible. The intensity of the visible incident light on the solution is measured with a photometre PMA 2200 (Solar Light C₀) being about 110 W m⁻² (photopic sensor PMA2130, spectral response 400–700 nm). In order to promote the adsorption–desorption equilibrium, before illumination, the suspension is stirred magnetically during 20 min in the dark. The total reaction time is 120 min for all tests. The concentration of MO during the photodegradation reactions are measured using UV–Visible spectroscopy, considering the main peak of MO centered at 465 nm. The Total Organic Carbon is monitored using a TOC Shimadzu 500 analyzer. Degrees of mineralization (%) are evaluated by TOC values over 2 h of irradiation, for all photo-assisted processes studied, using the formula:

$$\text{Mineralization Degree} = \left[1 - \frac{\text{Final TOC}}{\text{Initial TOC}} \right] \times 100$$

Results and discussion

The textural properties of the materials measured by N₂ adsorption–desorption are summarized in Table 1. These isotherms are of type IV (Fig. S1), with a hysteresis loop, signifying a mesoporous structure of the materials. On the other hand, the hysteresis loop is of the H3 type which corresponds to aggregates or agglomerates of particles forming slot-shaped pores, of non-uniform sizes. The results indicate that metal deposition on the TNR surface enables a slight decrease of the BET surface area of support. This phenomena can be explained by some fine porosity blocking upon the the formation of small clusters from the aggregation of gold and platinum particles.

Chemical composition of mono and bimetallic samples are shown in Table 2. We observed an important deposition rate of metals (Pt and Au) in the case of Au/TNR and Pt/TNR.

XPS analysis is carried out to verify the chemical, the electronic structure of catalysts and the valence states of various species present therein. Fig. S1 presents the Ti 2p, O 1s, Au 4f and Pt 4f XPS spectra of catalysts fitted with Gaussian distribution. The values of the binding energy are calibrated using C 1s peak (285.1 eV) as internal standard. The binding energies at 458.5 and 464.4 eV linked to the Ti 2p_{3/2} and Ti 2p_{1/2} of Ti (IV), respectively. In the case of O (1s) spectra (Fig. S2A), the peak at 531.9 eV is related to the –OH, while the binding energy at 529.8 eV corresponded to the Ti–O in which the valence of Ti is IV [21, 23]. In Fig. S2A, the Pt 4f peak of Pt/TNR contains four peaks related to the oxygenated Pt²⁺ and Pt⁴⁺ ions in the form of: PtO species (at 72.3 (4f_{7/2}) and 75.1 eV (4f_{5/2})), and PtO₂ species (73.8 (4f_{7/2}) and 77.2 eV (4f_{5/2})) [22–25]. The catalyst Au/TiO₂ (Fig. S2B) shows that the metallic state of gold (Au⁰) is the single metallic species on TNR surface. It presents two peaks at 84.0 and 87.6 eV linked to 4f_{7/2} and 4f_{5/2} [25–28], respectively.

Fig. S3 shows RD/UV–Vis spectrum of TNR. It shows an important absorption in the UV region which is linked to the charge transfer between tetrahedral Ti⁴⁺ species and oxygenated ligand like: O₂[–], O–H, O–Ti or even H₂O and to the Ti⁴⁺ cations in octahedral environment. After doping, the bands of the TNR are still present with a weak shift in comparison with TNR spectrum. This may be related to the interaction metal-support [27, 29]. Au/TNR catalyst presents an important absorption located around 562 nm (See Fig. S3); which is linked to the plasmonic resonance band produced by the metallic spherical gold nanoparticles; this band is influenced by the shape, the environment and the concentration of gold nanoparticles [28–35]. The adsorption in the visible region of the metalized TNR is attributed to the plasmonic band of the gold nanoparticles, this band improves the adsorption of the doped material in the visible region [31, 36].

The band gap energies can be obtained as the following equation $(\alpha h\nu)^n = k(h\nu - E_g)$, where α is the absorption coefficient, k is a constant, $h\nu$ is the photonic energy, E_g is the absorption band gap energy, n is 2 and 1/2 for a direct and indirect band gap semiconductor [32, 36–38]. Table 1 regroups the gap energy values of different materials. The results indicated that metalized TNR catalysts represent a red shift (Fig. S4). The band gap energies are located between 1.69 and 2.81 eV compared to the pristine TNR (2.05 eV).

Fig. S5 displays the XRD pattern of the TNR and metalized TNR. The presence of sodium tri-titanate having the formula: Na₂Ti₃O₇ (JCPDS 31-1329) is confirmed. This result is in agreement with those evoked in the literature, where several structures as A₂Ti₄O₉·H₂O and A₂Ti₈O₁₇ (A=H, Na, and K) types have been evoked resulting of a layer condensation pending the hydrothermal condensation [22]. The XRD spectra of metalized catalysts did not change significantly with the addition of Au and Pt nanoparticles, except that the diffraction peak located at $2\theta = 10.4^\circ$ shifted slightly to a smaller angle at $2\theta = 10.2^\circ$ in the case of metalized materials. The peak centered around 10.4° is due to the reflection of the (2 0 0) crystal plane and the shift toward a smaller diffraction angle is linked to the OH group in the alkaline TNR supports, which is attributed to the interlayer distance in the TNR wall [36, 38]. In addition, Au and Pt peaks are not detected because of the small metal amount used and dispersed nanoparticles.

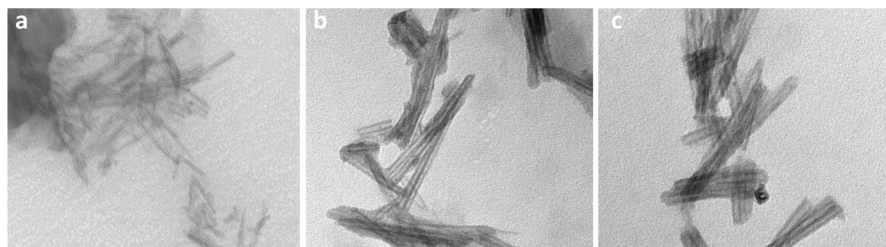


Fig. 1 TEM images of **a** TNR, **b** Pt/TNR and **c** Au/TNR

Fig. 1 shows the TEM images of the studied catalysts. We note that the TNR support has a hollow structure in the form of a nanorod having different dimensions. The length of the nanostructures varies from 20 to 120 nm while the width is almost homogeneous in the order of 8 nm. It is clear that doping does not cause any change in the structure of the dopant itself (Au or Pt). However, it is possible to detect some particles of the dopants in Fig. 1.

In conclusion of this part, we can say that the hydrothermal method made it possible to achieve the hollow nanorod structure. The TNR are doped with gold and platinum nanoparticles using deposition precipitation with urea or impregnation leading to a total and homogeneous deposition of the metal nanoparticles. The metallic nanoparticles have different oxidation states: Pt^{4+} , Pt^{2+} , Pt^0 , Au^{3+} , Au^0 . The materials obtained possess a large surface and an adequate gap energy which allows them to be applied in several types of reaction.

Photocatalytic activity

Fig. 2 shows conversion plots for photocatalytic transformation of MO under visible illumination using TNR, Au/TNR and Pt/TNR materials. After 120 min of reaction, the undoped-TNR shows a low degradation rate which does not exceed 30%. However, no mineralization of the MO has been shown as shown in Fig. 3. It is clear that the catalyst Pt/TNR presents the best performances with a total conversion after just 30 min under visible illumination. However, the photocatalyst Au/TiO₂ achieved only 30% of conversion after 60 min of reaction. The TOC analysis indicates a degree of mineralization around 70% for the platinum-based photocatalyst and slightly more than 40% for the others ones. The results demonstrated that Pt/TNR has a significant increase of the photodegradation rate as compared to the other catalysts.

Pt nanoparticles acts as an electron trap; electrons generated on the TNR surface under irradiation quickly move to the platinum nanoparticle surface and facilitate the separation effective of electrons and photogenerated holes, resulting an important improvement of the photocatalytic activity [37, 39].

In Fig. 4 shows the conversion plots of MO, using different amount of platinum: 0.5, 1, 2 and 5 wt% under visible irradiation. It is possible to observe that the transformation of MO for photocatalysts 1%Pt/TNR and 2%Pt/TNR remains unchanged; more than 94% of conversion after 30 min of visible-illumination is

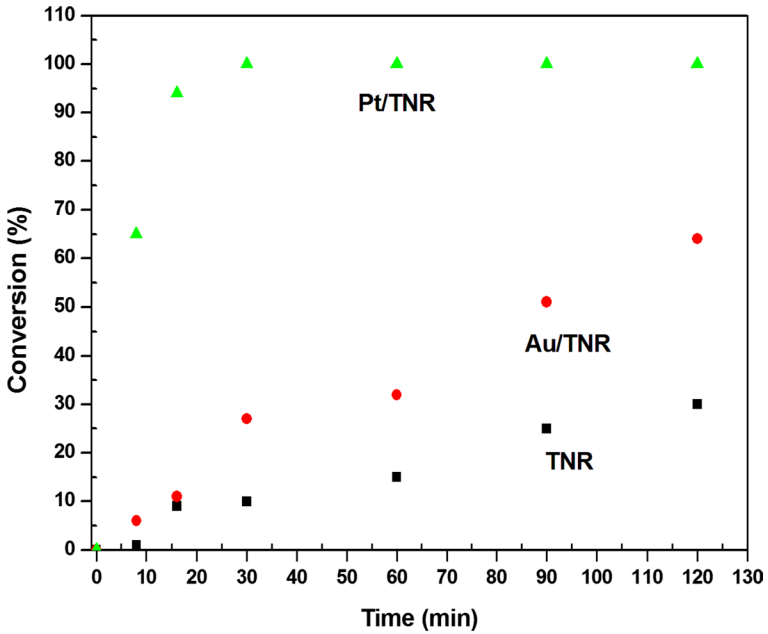


Fig. 2 Conversion plots for photocatalytic transformations of MO using, TNR, Au/TNR and Pt/TNR materials under visible-illumination

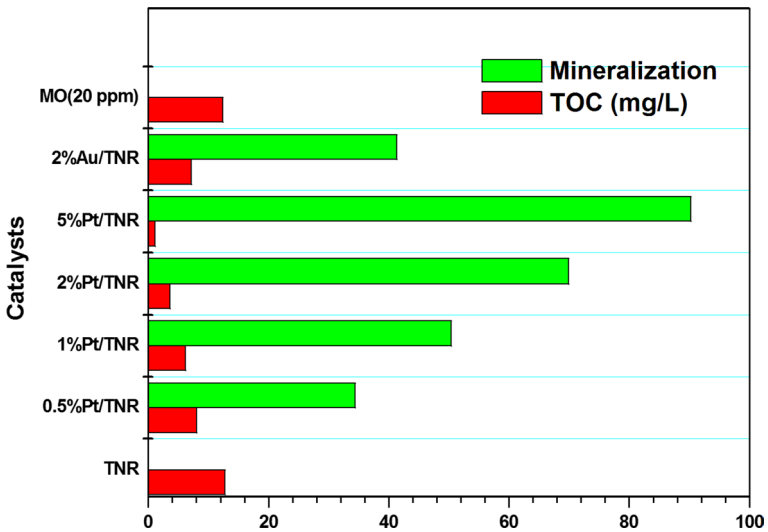


Fig. 3 The histograms of TOC and mineralization rates after 2 h of visible-irradiation of the different catalysts

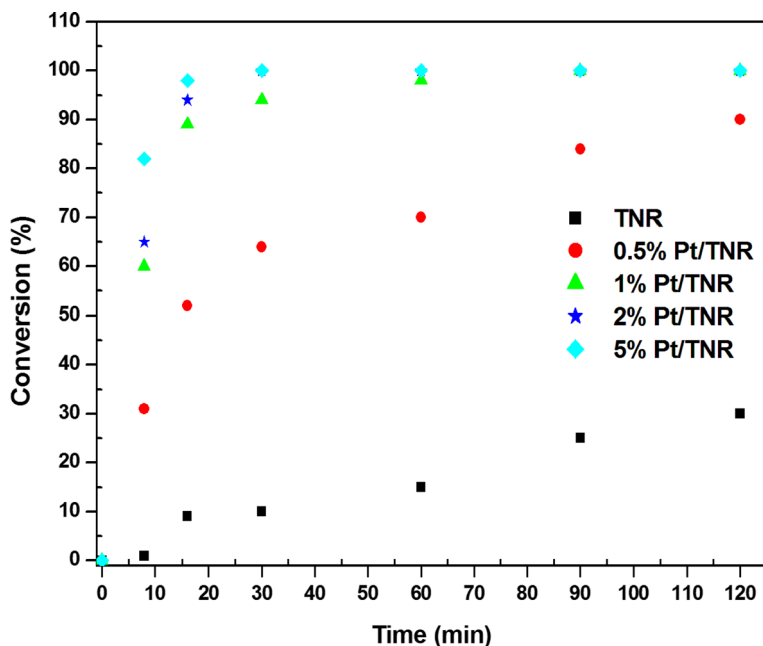


Fig. 4 Conversion plots for photocatalytic transformations of MO using x% Pt/TNR under UV-illumination

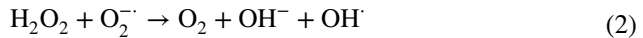
obtained. Though, with the photocatalyst at 5 wt% of Pt the conversion of MO achieved 98% after 20 min of irradiation. The TOC measurements indicate a degree of mineralization ranging 34, 50, 70 and 90% for the photocatalyst at 0.5, 1, 2 and 5% wt of Pt. At 2 wt%, the Pt plays a positive role of electron acceptor; more accepting centers receive increasing Pt doping. Therefore, the mineralization rate of methyl orange increases with the increase of Pt loading as is shown in Figs. 2 and 3.

We thought we studied the activity of TNR under UV irradiations in the presence of an oxidizer such as hydrogen peroxide.

The Pt/TNR catalyst showed significant stability via the photodegradation of the orange methyl under visible irradiation (Fig. S6). This suggests that this catalyst can find future applications on a large scale and in industry.

Influence of the activation of TNR with H_2O_2

In photocatalysis, addition of an oxidant such as H_2O_2 should be beneficial to the formation of hydroxyl radicals (OH^\bullet) as is shown in reactions 1, 2 and 3. The hydroxyl radical is a dominant and strong oxidization species in photocatalytic process. It is able to oxidize a variety of organic substances completely on the surface of TiO_2 illuminated using UV light. Therefore, addition of H_2O_2 should facilitate the generation of OH^\bullet and consequently promote the photodegradation process [39–42].



In this part of the study, an initial concentration of H_2O_2 is added in presence of TNR and P25 at a concentration of 5 mL g^{-1} . Then, the samples are leave until the adsorption equilibrium is reached. A yellow-colored complex appeared for the samples after H_2O_2 addition and a stronger coloration is observed for TNR materials. Photocatalytic tests of MO degradation are carried in the same conditions of illumination as previously (See experimental section). The results of the conversion plots for photocatalytic transformation of MO under UV-illumination using TNR- H_2O_2 and P25- H_2O_2 samples are represented in Fig. 5.

Fig. 5 shows the conversion plots for photocatalytic transformation of MO under UV-illumination using TNR, TNR pretreated by H_2O_2 , P25 and P25 pretreated by H_2O_2 . The figure shows clearly a positive effect of H_2O_2 addition for both samples especially in the first min of reaction. H_2O_2 is mentioned as one of the intermediate species in titania-based photocatalytic reactions [40, 41, 43, 44]. The adsorption capacity of H_2O_2 on titania depends on the structure and on the

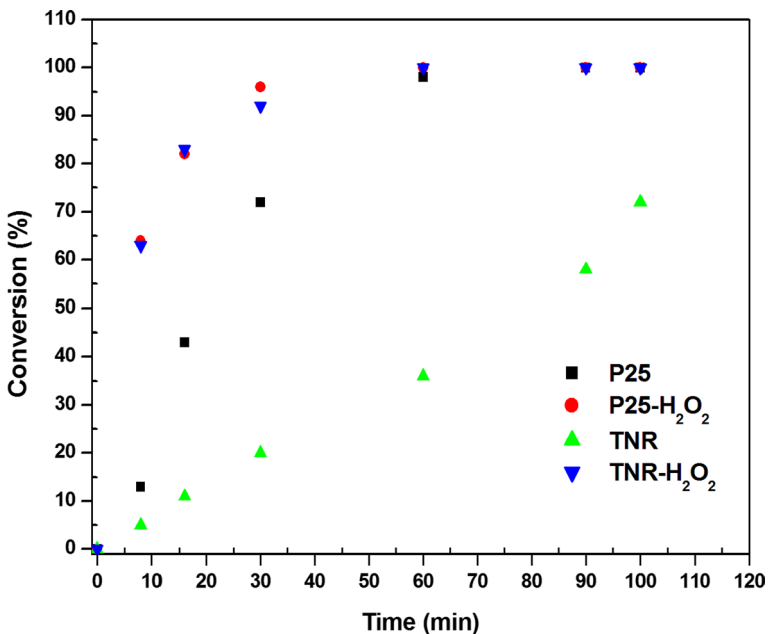


Fig. 5 Conversion plots for photocatalytic transformations of MO using P25, P25- H_2O_2 , TNR and TNR- H_2O_2 under UV-illumination

catalysts surface area and the necessity of interaction between catalyst surface and H_2O_2 to be degraded [43, 45].

A yellow color appeared when the TNR are treated with H_2O_2 . The intensity of the coloration depended on the concentration of the H_2O_2 solution and on the specific surface area of the samples as already observed by different authors. Several works show that the yellow complex corresponds to Ti-peroxo species formed between Ti(IV) and H_2O_2 [45–49]. The Ti- η^2 -peroxide is the main Ti-peroxo complex formed on the surface of rutile TiO_2 whereas Ti- μ -peroxide is mainly generated on the anatase phase [47, 48]. The Ti-peroxo complexes proposed exists in three forms as is shown in Fig. S7.

Conclusion

The metallization of TNR by platinum and gold can improve the visible absorption and photocatalytic activity of the resulting catalysts. Pt/TNR prepared by impregnation method shows the most important phodegradation of MO. It can be degraded totally within 30 min under visible irradiation. Also, with the increase of Pt amount on the catalysts the photoderagation is improved which is related to the increase of active sites. However, gold catalyst showed lower activity in the MO degradation in comparison with platinum catalysts. Finally, we can improve the photodegradation of TNR by H_2O_2 activation which leads to the formation of more OH^{\bullet} radicals.

Supplementary Information The online version contains supplementary material available at <https://doi.org/10.1007/s11144-023-02460-6>.

Acknowledgements The authors extend their appreciation to the Deanship of Scientific Research at King Khalid University for funding this work through large group Research project under Grant Number RGP2/47/44.

Author contributions All authors contributed to the study conception and redaction. Material preparation, data collection and analysis are performed by all authors. The first draft of the manuscript is written and commented by Sanaa Ben Moussa.

Funding Not applicable.

Data availability Not applicable.

Declarations

Competing interests The authors declare no competing interests.

Ethical approval Not applicable.

References

1. Lachheb H, Puzenat E, Houas A, Ksibi M, Elaloui E, Guillard C, Herrmann J-M (2002) Photocatalytic degradation of various types of dyes (Alizarin S, Crocein Orange G, Methyl Red, Congo Red, Methylene Blue) in water by UV-irradiated titania. *Appl Catal B* 39:75–90

- Serpone N (2018) Heterogeneous photocatalysis and prospects of TiO₂-based photocatalytic DeNO_xing the atmospheric environment. *Catalysts* 8:553
- Saadati M, Akhavan O, Fazli H (2021) Single-layer MoS₂-MoO_{3-x} heterojunction nanosheets with simultaneous photoluminescence and co-photocatalytic features. *Catalysts* 11:1445
- Styliidi M, Kondarides DI, Veyrikios XE (2003) Pathways of solar light-induced photocatalytic degradation of azo dyes in aqueous TiO₂ suspensions. *Appl Catal B* 40:271–286
- Chong MN, Jin B, Chow CW, Saint C (2010) Recent developments in photocatalytic water treatment technology: a review. *Water Res* 44:2997–3027
- Cai C, Zhang Z, Liu J, Shan N, Zhang H, Dionysiou DD (2016) Visible light-assisted heterogeneous Fenton with ZnFe₂O₄ for the degradation of Orange II in water. *Appl Catal B* 182:456–468
- Akpan UG, Hameed BH (2009) Parameters affecting the photocatalytic degradation of dyes using TiO₂-based photocatalysts: a review. *J Hazard Mater* 170:520–529
- Qin L-Z, Liao B, Dong X-L, Wu X-Y, Hou X-G, Liu A-D (2009) Ag/Fe:TiO₂ nano-catalysts prepared by Fe ion implantation and Ag nanoparticle deposition by electron beam irradiation. *Nucl Instrum Methods Phys Res Sect B* 267:1077–1080
- Fernandes A, Makoś P, Wang Z, Boczkaj G (2020) Synergistic effect of TiO₂ photocatalytic advanced oxidation processes in the treatment of refinery effluents. *Chem Eng J* 391:123488
- Ebrahimi M, Akhavan O (2022) Nanomaterials for photocatalytic degradations of analgesic, mucolytic and anti-biotic/viral/inflammatory drugs widely used in controlling SARS-CoV-2. *Catalysts* 12:667
- Poyatos JM, Muñoz M, Almecija M, Torres J, Hontoria E, Osorio F (2010) Advanced oxidation processes for wastewater treatment: state of the art. *Water Air Soil Pollut* 205:187–204
- Hernández R, Durón-Torres SM, Esquivel K, Guzmán C (2017) Microwave assisted sol-gel synthesis and characterization of M-TiO₂ (M= Pt, Au) photocatalysts. Characterization of metals and alloys. Springer International Publishing, Cham, pp 183–189
- Macwan D, Dave PN, Chaturvedi S (2011) A review on nano-TiO₂ sol-gel type syntheses and its applications. *J Mater Sci* 46:3669–3686
- Chen X, Mao SS (2007) Titanium dioxide nanomaterials: synthesis, properties, modifications, and applications. *Chem Rev* 107:2891–2959
- Liü D, Li Z, Wang W, Wang G, Liú D (2016) Hematite doped magnetic TiO₂ nanocomposites with improved photocatalytic activity. *J Alloys Compd* 654:491–497
- Lei X, Xue X, Yang H (2014) Preparation and characterization of Ag-doped TiO₂ nanomaterials and their photocatalytic reduction of Cr (VI) under visible light. *Appl Surf Sci* 321:396–403
- Liu L, Gao F, Zhao H, Li Y (2013) Tailoring Cu valence and oxygen vacancy in Cu/TiO₂ catalysts for enhanced CO₂ photoreduction efficiency. *Appl Catal B* 134:349–358
- Akhavan O (2009) Lasting antibacterial activities of Ag-TiO₂/Ag/a-TiO₂ nanocomposite thin film photocatalysts under solar light irradiation. *J Colloid Interface Sci* 336:117–124
- Rosseler O, Shankar MV, Du Karkmaz-Le M, Schmidlin L, Keller N, Keller V (2010) Solar light photocatalytic hydrogen production from water over Pt and Au/TiO₂ (anatase/rutile) photocatalysts: influence of noble metal and progen promotion. *J Catal* 269:179–190
- Maicu M, Hidalgo M, Colón G, Navío JA (2011) Comparative study of the photodeposition of Pt, Au and Pd on pre-sulphated TiO₂ for the photocatalytic decomposition of phenol. *J Photochem Photobiol A* 217:275–283
- Zou X, Dong Y, Zhang X, Cui Y (2016) Synthesize and characterize of Ag₃VO₄/TiO₂ nanorods photocatalysts and its photocatalytic activity under visible light irradiation. *Appl Surf Sci* 366:173–180
- Liu J, Li Y, Ke J, Wang S, Wang L, Xiao H (2018) Black NiO-TiO₂ nanorods for solar photocatalysis: Recognition of electronic structure and reaction mechanism. *Appl Catal B* 224:705–714
- Meng X-D, Wang D-Z, Liu J-H, Zhang S-Y (2004) Preparation and characterization of sodium titanate nanowires from brookite nanocrystallites. *Mater Res Bull* 39:2163–2170
- Watanabe M, Uchida M, Motoo S (1987) Preparation of highly dispersed Pt + Ru alloy clusters and the activity for the electrooxidation of methanol. *J Electroanal Chem Interfacial Electrochem* 229:395–406
- Arico A, Shukla A, Kim H, Park S, Min M, Antonucci V (2001) An XPS study on oxidation states of Pt and its alloys with Co and Cr and its relevance to electroreduction of oxygen. *Appl Surf Sci* 172:33–40
- Parkinson C, Walker M, McConville C (2003) Reaction of atomic oxygen with a Pt (111) surface: chemical and structural determination using XPS, CAICISS and LEED. *Surf Sci* 545:19–33
- Kim M-J, Na H-J, Lee KC, Yoo EA, Lee M (2003) Preparation and characterization of Au-Ag and Au-Cu alloy nanoparticles in chloroform. *J Mater Chem* 13:1789–1792
- Si R, Flytzani-Stephanopoulos M (2008) Shape and crystal-plane effects of nanoscale ceria on the activity of Au-CeO₂ catalysts for the water-gas shift reaction. *Angew Chem* 120:2926–2929

29. Gluhoi AC, Bogdanchikova N, Nieuwenhuys BE (2005) Alkali (earth)-doped Au/Al₂O₃ catalysts for the total oxidation of propene. *J Catal* 232:96–101
30. Sangpour P, Akhavan O, Moshfegh A, Roozbehi M (2007) Formation of gold nanoparticles in heat-treated reactive co-sputtered Au–SiO₂ thin films. *Appl Surf Sci* 254:286–290
31. Ameer N, Bedrane S, Bachir R, Choukchou-Braham A (2013) Influence of nanoparticles oxidation state in gold based catalysts on the product selectivity in liquid phase oxidation of cyclohexene. *J Mol Catal A: Chem* 374–375:1–6
32. Ameer N, Berrichi A, Bedrane S, Bachir R (2014) Preparation and characterization of Au/Al₂O₃ and Au–Fe/Al₂O₃ materials, active and selective catalysts in oxidation of cyclohexene. *Adv Mater Res* 856:48–52
33. Simakov A, Tuzovskaya I, Bogdanchikova N, Pestryakov A, Avalos M, Farias M, Smolentseva E (2008) Influence of sodium on activation of gold species in Y–zeolites. *Catal Commun* 9:1277–1281
34. Eustis S, El-Sayed MA (2006) Why gold nanoparticles are more precious than pretty gold: noble metal surface plasmon resonance and its enhancement of the radiative and nonradiative properties of nanocrystals of different shapes. *Chem Soc Rev* 35:209–217
35. Karooby E, Granpayeh N (2019) Potential applications of nanoshell bow-tie antennas for biological imaging and hyperthermia therapy. *Opt Eng* 58:065102–065102
36. Pestryakov A, Tuzovskaya I, Smolentseva E, Bogdanchikova N, Jentoft FC, Knop-Gericke A (2005) Formation of gold nanoparticles in zeolites. *Int J Mod Phys B* 19:2321–2326
37. Jiang H, Meng X, Dai H, Deng J, Liu Y, Zhang L, Zhao Z, Zhang R (2012) High-performance porous spherical or octapod-like single-crystalline BiVO₄ photocatalysts for the removal of phenol and methylene blue under visible-light illumination. *J Hazard Mater* 217:92–99
38. Ameer N, Bachir R (2020) Study of 1D titanate-based materials–new modification of the synthesis procedure and surface properties–recent applications. *ChemistrySelect* 5:1164–1185
39. Anpo M, Takeuchi M (2003) The design and development of highly reactive titanium oxide photocatalysts operating under visible light irradiation. *J Catal* 216:505–516
40. Irmak S, Kusvuran E, Erbatur O (2004) Degradation of 4-chloro-2-methylphenol in aqueous solution by UV irradiation in the presence of titanium dioxide. *Appl Catal B* 54:85–91
41. Konstantinou IK, Albanis TA (2004) TiO₂-assisted photocatalytic degradation of azo dyes in aqueous solution: kinetic and mechanistic investigations: a review. *Appl Catal B* 49:1–14
42. Wang Y, Hong C-S (1999) Effect of hydrogen peroxide, periodate and persulfate on photocatalysis of 2-chlorobiphenyl in aqueous TiO₂ suspensions. *Water Res* 33:2031–2036
43. Navío JA, Colón G, Sánchez-Soto PJ, Macías M (1997) Effects of H₂O₂ and SO₄²⁻-species on the crystalline structure and surface properties of ZrO₂ processed by alkaline precipitation. *Chem Mater* 9:1256–1261
44. Hirakawa T, Nosaka Y (2002) Properties of O₂^{•-} and OH[•] formed in TiO₂ aqueous suspensions by photocatalytic reaction and the influence of H₂O₂ and some ions. *Langmuir* 18:3247–3254
45. Sahel K, Elsellami L, Mirali I, Dappozze F, Bouhent M, Guillard C (2016) Hydrogen peroxide and photocatalysis. *Appl Catal B* 188:106–112
46. Boonstra A, Mutsaers C (1975) Adsorption of hydrogen peroxide on the surface of titanium dioxide. *J Phys Chem* 79:1940–1943
47. Ohno T, Masaki Y, Hirayama S, Matsumura M (2001) TiO₂-photocatalyzed epoxidation of 1-decene by H₂O₂ under visible light. *J Catal* 204:163–168
48. Li X, Chen C, Zhao J (2001) Mechanism of photodecomposition of H₂O₂ on TiO₂ surfaces under visible light irradiation. *Langmuir* 17:4118–4122
49. Pavel CC, Park S-H, Dreier A, Tesche B, Schmidt W (2006) Structural defects induced in ETS-10 by postsynthesis treatment with H₂O₂ solution. *Chem Mater* 18:3813–3820

Publisher's Note Springer Nature remains neutral with regard to jurisdictional claims in published maps and institutional affiliations.

Springer Nature or its licensor (e.g. a society or other partner) holds exclusive rights to this article under a publishing agreement with the author(s) or other rightsholder(s); author self-archiving of the accepted manuscript version of this article is solely governed by the terms of such publishing agreement and applicable law.